$$F_i = f_i L_i^2 L_0/s - G^* L_i^3 + G^* L_0^3$$
$$\Phi_i = F_i(G^{*0}, L_0^0, f_i, L_i) \quad \text{(A-7)}$$

For the birefringence data, procedures exactly analogous to A-6 and A-7 were followed, based on eq 4 and 2

$$F_i = \lambda_0 L_i^{3/2} L_0^{3/2} \varphi_i/(180\ \mathrm{d}(L_i^3 - L_0^3)) - A_1^* - A_2^* L_0/L_i = 0 \quad \text{(A-6a)}$$

and

$$F_i = \lambda_0 L_i^{3/2} L_0^{3/2} \varphi_i/(180\ \mathrm{d}) - A^* L_i^3 + A^* L_0^3 \quad \text{(A-7a)}$$

with $m_{xi} = m_\varphi = 15$ min, $m_{yi} = m_L = 0.005$ cm.

In all cases the iteration converges in about two to three steps for eq A-7 and four to five steps for eq A-6. In most cases (except in ethylene glycol as diluent), the two-parameter Mooney–Rivlin-type equations (A-6) describe the results better than the Gaussian-type equations (A-7), as can be seen from Figure 12. It should be noted that the best values for L_0 according to (A-7) and (A-6) do not differ more than the experimental error in L_i. The value of C_2^* is, however, very sensitive to the value of L_0 used. For $\Lambda < 1.5$ typical uncertainties in the final constants are G^* ±5%, C_1^* ±10%, and C_2^* ±20%.

The procedure outlined in this Appendix represents the best possible way of treating the data; by means of eq A-4 the various measured quantities are given proper statistical weight, *i.e.*, $f_i L_i$ values close to L_0 are weighted less than those far away from L_0, in the case of fitting to eq A-6 (for $1 < \Lambda < 1.5$, p_i varies thousandfold). For eq A-7 the statistical weights do not vary very much (for $1 < \Lambda < 1.5$, p_i varies less than twofold in opposite directions).

Rheo-Optics of Poly(2-hydroxyethyl methacrylate) Gels. II. Effect of Cross-Linking Density and Stage of Dilution during Network Formation

M. Ilavsky and W. Prins*

Department of Chemistry, Syracuse University, Syracuse, New York 13210.
Received March 30, 1970

ABSTRACT: In order to study the structure of poly(2-hydroxyethyl methacrylate) networks in water, a series of hydrogels was prepared in which the stage of dilution during copolymerization was varied (concentration of cross-linker c 0.065 × 10^{-4} mol/cm³, 0, 20, 40, 46.5, and 47% H_2O) as well as a series in which the cross-linker concentration was varied (0% water, c 0.086–2.06 10^{-4} mol/cm³). Rheo-optical studies were conducted on samples swollen to equilibrium in water at $T = 25°$ in the rubbery region. The anisotropic light scattering increases with c and decreases with the per cent H_2O during network formation; in all cases a certain amount of long-range orientation correlation exists over thousands of ångströms. Stress and birefringence relaxation data at various elongations (Λ = 1–1.6) were found to be separable in an elongation- and time-dependent factor. The viscoelastic nature of the stress–time dependence allowed the construction of a superposed curve using an apparent molecular weight between cross-links as reduction variable ($M_{app} = RTq^{-1/3}\rho_d/(C_1^* + C_2^*)$ where ρ_d = density of the dry network). The time dependence of the birefringence was found to be slower than that of the stress, with the difference between them vanishing at $M_{app} \leq 10{,}000$ g/mol. The extrapolated equilibrium stress and birefringence fit a Mooney–Rivlin representation better than a Gaussian. The C_2^*/C_1^* ratio (even after Gaussian correction to the dry state) increases with the per cent H_2O during network formation (C_2^* is about constant), but decreases rapidly with increasing c and vanishes at $M_{app} \leq 10{,}000$. The equilibrium stress–optical coefficient, which is essentially independent of Λ, rapidly decreases about ninefold with decreasing M_{app}. Upon analysis, all the above results fit the picture of a structured network as outlined in a previous paper. Because of the amphiphilic nature of the polymer, specific interaction with water may well lead to a certain type of mesomorphic ordering in the network.

Poly(2-hydroxyethyl methacrylate) networks swollen in aqueous media are currently in use as biomedical materials.[1] The structure of such PHEMA hydrogels depends very markedly on the stage of dilution during cross-linking. Visually clear gels are obtained if the water content during network formation is less than about 45 wt %. Above this critical dilution turbid gels and eventually white spongy materials are formed. The turbidity above the critical dilution is caused by the poor compatibility of the polymer with water. Cross-linked gels prepared by copolymerization below the critical dilution all swell to about 45% water—virtually independent of the cross-linking density—when they are submerged in pure water. A normal dependence of the swelling upon the cross-linking density is found[2] when one employs a good diluent as, for example, ethylene glycol.

It has been argued in previous communications[3,4] that especially in water, but also in other hydrogen-bonding diluents,[4] a certain amount of diluent-induced ordering may exist. It seems quite conceivable that

(1) O. Wichterle and D. Lim, *Nature (London)*, **185**, 117 (1960).

(2) J. Hasa and M. Ilavsky, *Collect. Czech. Chem. Commun.*, **34**, 2189 (1969).

(3) J. H. Gouda, K. Povodator, T. C. Warren, and W. Prins, *Polym. Lett.*, in press.

(4) M. Ilavsky and W. Prins, *Macromolecules*, **3**, 415 (1970).

inter- and intramolecular alternating hydrophilic and hydrophobic layers are formed by parts of the strongly amphiphilic PHEMA chains. Because the gels are chemically cross-linked such layered regions will be limited in size and will probably be dependent on the cross-linking density. In an analogy with similarly amphiphilic soap systems, it has been suggested to designate the resulting structure as micromesomorphic in nature.[3]

In view of the above considerations a series of hydrogels was prepared in which the stage of dilution during copolymerization was varied, as well as a series in which the cross-linker concentration was varied. The samples were swollen to equilibrium in water and investigated in water by means of stress and birefringence relaxation in elongation as well as by means of small-angle light scattering, the objective being to uncover the relation between the mechanical properties and the structure of the gels. As in the preceding article[4] the stress $\sigma(\Lambda,t)$ and birefringence $\Delta n(\Lambda,t)$ relaxation could be described very well by

$$\begin{aligned} \sigma(\Lambda,t) &= \sigma_e(\Lambda)\sigma_2(t) \\ \Delta n(\Lambda,t) &= \Delta n_e(\Lambda)\Delta n_2(t) \end{aligned} \tag{1}$$

where Λ is the elongation ratio.

From $\sigma_2(t)$ and $\Delta n_2(t)$ mechanical and optical relaxation spectra $h^{(m)}$ and $h^{(o)}$ could be derived[4]

$$\begin{aligned} \sigma_2(t) &= 1 + \int_{-\infty}^{+\infty} h^{(m)} e^{-t/\tau}\, d \log \tau \\ \Delta n_2(t) &= 1 + \int_{-\infty}^{+\infty} h^{(o)} e^{-t/\tau}\, d \log \tau \end{aligned} \tag{2}$$

In the case that there exists only a Rouse-type configurational relaxation of the chains between cross-links, one has $h^{(o)} = h^{(m)}$ and thus a time-dependent stress–optical coefficient.[5] The spectra of PHEMA gels in various diluents, including water, were found not to be identical;[4] the causes for this were traceable to a (re)-formation of interchain correlations, after the (partial) destruction of such correlations upon the imposition of a deformation (see also below).

The equilibrium behavior was described in terms of Mooney–Rivlin equations[4]

$$\begin{aligned} \sigma_e &= (C_1^* + C_2^*/\Lambda)(\Lambda^2 - \Lambda^{-1}) \\ \Delta n_e &= (A_1^* + A_2^*/\Lambda)(\Lambda^2 - \Lambda^{-1}) \end{aligned} \tag{3}$$

which means that there are deviations from the classical equilibrium equations of Gaussian networks

$$\begin{aligned} \sigma_e &= G_d^* q^{-1/3}[\Lambda^2 - \Lambda^{-1}] = G^*[\Lambda^2 - \Lambda^{-1}] \\ \Delta n_e &= A_d^* q^{-1/3}[\Lambda^2 - \Lambda^{-1}] = A^*[\Lambda^2 - \Lambda^{-1}] \end{aligned} \tag{4}$$

where q is the volume degree of swelling prior to the deformation, which is essentially the same as that after deformation,[4] and

$$\begin{aligned} G_d^* &= A q_0^{-2/3} \nu^* RT \\ A_d &= (G_d^*/kT)(2\pi/45)(\bar{n}^2 + 2)^2 \bar{n}^{-1} \Delta\alpha_c \end{aligned} \tag{5}$$

with ν^* the number of moles of effective network chains per cubic centimeter of dry network, A a numerical factor reflecting a minor ambiguity in the derivation of eq 4, and $\bar{n}$ the average refractive index of the gel. The quantity $\Delta\alpha_c$ is the optical anisotropy per chain segment and $q_0^{-2/3}$ is given by[6]

$$q_0^{-2/3} = \frac{\langle r^2\rangle_d}{\langle r^2\rangle_{os}} = \frac{\langle r^2\rangle_d \langle r^2\rangle_c}{\langle r^2\rangle_c \langle r^2\rangle_{os}} \approx q_c^{-2/3} \tag{6}$$

In eq 6 the $\langle r^2\rangle$ values refer to average chain dimensions in the dry state (d), unperturbed (swollen) state (os), and immediately after network formation (c), respectively. As a reasonable approximation one often puts $\langle r^2\rangle_c = \langle r^2\rangle_{os}$ so that the "front factor" $q_0^{-2/3}$ equals $q_c^{-2/3}$, where q_c represents the stage of dilution during network formation, expressed as volume degree of swelling. According to the Gaussian equations (4 and 5), the equilibrium stress optical coefficient

$$C_e = \Delta n_e/\sigma_e = A^*/G^* = (1/kT)(2\pi/45)(\bar{n}^2 + 1)^2 \bar{n}^{-1} \Delta\alpha_c \tag{7}$$

should be independent of the stage of dilution during network formation (q_c) and independent of the number of chains in the network (ν^*). We will see below that eq 7 is not at all obeyed in PHEMA hydrogels.

Direct structural information is obtained from the small-angle light scattering of the unstrained hydrogels. The angular dependence of the scattering can be analyzed in terms of long-range correlation functions or alternatively by reference to a model. For a network which is thought to consist of an amorphous Gaussian matrix in which a number of anisotropic rodlike regions (interchain correlated regions) are embedded, one has[4] for the case of incident light with polarization perpendicular to the (horizontal) scattering plane, and horizontally polarized scattered light, the following relation for the scattered intensity extrapolated to zero scattering angle, θ

$$[H_v]_{\theta=0} = (16\pi^4/15\lambda_0^4)[\phi_{an}(\Delta\alpha_{an}^i)^2 V_{an} + \phi_c(\Delta\alpha_c^i)^2 V_c + \phi_x(\Delta\alpha_x^i)^2 V_x] \tag{8}$$

In this equation, λ_0 is the vacuum wavelength of the light; ϕ_{an}, ϕ_c, and ϕ_x are the volume fractions of anisotropic regions, chain segments, and cross-links respectively ($\phi_{an} + \phi_c + \phi_x = 1$); and $\Delta\alpha_{an}^i$, $\Delta\alpha_c^i$, and $\Delta\alpha_x^i$ are the respective intrinsic anisotropies per unit volume, and V_{an}, V_c, V_x are the respective volumes. Of the various possible light-scattering components (*e.g.*, V_v, H_h, H_v, in general $R^{\parallel}$ and $R^{\perp}$, see ref 7), H_v (or more generally $R^{\perp}$) is the only "pure" component, *i.e.*, it depends only on the local anisotropy and is independent of the refractive index. The other components all reflect differences in local refractive index as well as in local birefringence, and are therefore less amenable to interpretation.

Experimental Section

Preparation of Samples. Copolymerization of 2-hydroxyethyl methacrylate (HEMA) with ethylene glycol dimethacrylate (EGMA) was carried out in glass or Teflon molds in the presence of varying amounts of water, at 55°, using

(5) B. E. Read, *Polymer*, 3, 143 (1962).

(6) See, *e.g.*, K. Dušek and W. Prins, *Fortschr. Hochpolym.-Forsch.*, 6, 1 (1969).

(7) J. H. Gouda and W. Prins, *J. Polym. Sci., Part A-2*, in press.

TABLE I
OPTICAL AND MECHANICAL CHARACTERISTICS OF PHEMA HYDROGELS[a]

	Sample no.												
	1	2	3	4	5	6	7	8	9	10	11	12	13
% H_2O at polym	47.0	46.5	40.0	20.0	0	0	0	0	0	0	0	0	0
10^5c, mol cm^{-3}	0.65	0.65	0.65	0.65	0.65	0.86	1.36	1.87	2.44	3.41	5.44	10.41	20.58
q	1.89	1.89	1.88	1.85	1.86	1.85	1.84	1.82	1.82	1.79	1.82	1.76	1.68
$10^{-6}G^*$ (5 min)	0.89	0.94	1.07	1.33	1.35	1.55	1.84	1.98	2.13	2.54	3.36	4.84	8.38
$10^{-6}G^*$ (1 hr)	0.75	0.81	0.92	1.20	1.25	1.45	1.76	1.88	2.06	2.47	3.29	4.80	8.37
$10^{-6}G^*$ (∞)	0.30	0.34	0.57	0.88	0.92	1.18	1.49	1.76	1.96	2.41	3.25	4.77	8.37
$10^{-6}C_1^*$ (5 min)	0.52	0.53	0.63	0.89	0.94	1.14	1.35	1.66	1.86	3.33	3.19		
$10^{-6}C_1^*$ (1 hr)	0.40	0.47	0.53	0.81	0.77	1.02	1.20	1.54	1.80	2.26	3.12		
$10^{-6}C_1^*$ (∞)	0.18	0.23	0.29	0.50	0.64	0.84	1.01	1.50	1.72	2.15	3.11		
$10^{-6}C_2^*$ (5 min)	0.55	0.58	0.62	0.60	0.60	0.60	0.71	0.52	0.35	0.30	0.15		
$10^{-6}C_2^*$ (1 hr)	0.51	0.48	0.54	0.53	0.55	0.60	0.65	0.48	0.34	0.32	0.13		
$10^{-6}C_2^*$ (∞)	0.17	0.16	0.43	0.51	0.54	0.52	0.64	0.50	0.33	0.27	0.09		
C_2^*/C_1^* (5 min)	1.06	1.09	0.98	0.67	0.64	0.53	0.53	0.31	0.19	0.13	0.05		
C_2^*/C_1^* (1 hr)	1.28	1.02	1.02	0.65	0.71	0.59	0.54	0.31	0.19	0.14	0.04		
C_2^*, C_1^* (∞)	0.94	0.70	1.48	1.02	0.84	0.62	0.63	0.33	0.19	0.13	0.03		
10^5A^* (5 min)	4.44	4.13	2.50	2.50	2.40	2.44	2.58	2.57	2.32	3.02	2.95	3.26	4.52
10^5A^* (1 hr)	3.85	3.38	2.22	2.35	2.28	2.28	2.55	2.49	2.26	2.93	2.88	3.25	4.52
10^5A^* (∞)			1.72	2.12	1.78	2.07	2.29	2.45	2.20	2.86	2.83	3.22	4.52
$10^5A_1^*$ (5 min)	3.25	0.90	0.91	1.35	1.70	1.61	1.58	1.71	1.62	2.17			
$10^5A_1^*$ (1 hr)	1.40	0.70	0.76	1.29	1.45	1.46	1.50	1.68	1.55	2.04			
$10^5A_1^*$ (∞)			0.72	1.18	1.30	1.27	1.21	1.67	1.52	2.00			
$10^5A_2^*$ (5 min)	1.73	4.5	2.19	1.64	0.90	1.15	1.38	1.17	1.86	0.96			
$10^5A_2^*$ (1 hr)	3.28	4.1	2.03	1.39	0.75	1.17	1.31	1.05	0.87	1.03			
$10^5A_2^*$ (∞)			1.42	1.31	0.53	1.00	1.08	1.02	0.84	1.00			
A_2^*/A_1^* (5 min)	0.53	5.0	2.41	1.21	0.54	0.71	0.87	0.68	0.53	0.44			
A_2^*/A_1^* (1 hr)	2.34	5.8	2.67	1.07	0.59	0.80	0.87	0.63	0.56	0.50			
A_2^*/A_1^* (∞)			1.97	1.11	0.41	0.79	0.90	0.65	0.55	0.50			
$10^{11}\Delta n\sigma^{-1}$ (5 min)	4.72	4.64	2.34	1.88	1.70	1.53	1.40	1.30	1.09	1.14	0.88	0.67	0.54
$10^{11}\Delta n\sigma^{-1}$ (1 hr)	4.71	4.63	2.41	1.96	1.79	1.57	1.45	1.32	1.10	1.17	0.88	0.68	0.54
$10^{11}\Delta n\sigma^{-1}$ (∞)			3.02	2.41	1.95	1.73	1.57	1.39	1.12	1.17	0.87	0.68	0.54

[a] G^*, C_1^*, C_2^*, and σ are all in dyn/cm^2.

1×10^{-2} mol/l. of isopropyl percarbonate as radical initiator. In one series the cross-linker concentration was kept constant at 0.065×10^{-4} mol/cm^3, but dilutions of 0, 20, 40, 46.5, and 47% by weight were employed. In the second series no water was added but the cross-linker concentrations were c 10^4 mol/cm^3 = 0.086, 0.136, 0.187, 0.244, 0.341, 0.544, 1.041, and 2.058. After extraction with methanol or water, the samples were swollen to equilibrium in water. Volumes and densities in dry and swollen states were determined and adjusted as before.[4] The volume degree of swelling q obtained in this way is shown in Table I. Strips of about $50 \times 10 \times 2$ mm^3 were cut for use in the various experiments.

Photoelasticity and Light Scattering. In the preceding article[4] the instrumentation and experimental procedure for measuring $\sigma(\Lambda,t)$ and $\Delta n(\Lambda,t)$ during stress relaxation at various elongation ratios Λ has been described. The birefringence is measured as a transmitted light intensity which is converted to the extinction angle $\varphi(t)$. The force $f(t)$ was read off a force transducer, the length was obtained by a cathetometer. Experiments were normally carried out over 2 hr for about ten different elongation ratios; two or three experiments per sample were extended over 5–8 hr.

Small-angle light-scattering data were taken at scattering angles $2° \leq \theta \leq 30°$, employing vertically polarized incident light and horizontally polarized scattered light (H_v) as well as other combinations (V_v, H_h). A detailed description of the conversion of measured intensities to Rayleigh ratios, R_θ, can be found elsewhere.[8] The refractive indices, n_g, were measured in an Abbe refractometer.

(8) A. E. M. Keyzers, J. J. van Aartsen, and W. Prins, *J. Appl. Phys.*, **36**, 2874 (1965).

Results

As before,[4] force and extinction angle could be written as (see eq 1) $f(\Lambda,t) = f_e(\Lambda)f_2(t)$ and $\varphi(\Lambda,t) = \varphi_e(\Lambda) \cdot \varphi_2(t)$, with $f_e(\Lambda)$ and $\varphi_e(\Lambda)$ being the extrapolated equilibrium values. Figure 1 gives an example of the correctness of this separation ($\log f(\Lambda,t)$ and $\log \varphi(\Lambda,t)$ *vs.* $\log t$ yield parallel lines at various elongations Λ). In order to avoid hysteresis each strip was given a recovery time of at least ten times longer than the time used in the experiment. The time dependencies could be approximated very well by[4]

$$f_2(t) = 1 + [t/t_0^{(m)}]^{-m^{(m)}}$$
$$\varphi_2(t) = 1 + [t/t_0^{(o)}1]^{-m^{(o)}} \quad (9)$$

where t_0 and m are constants, labeled (m) for the mechanical and (o) for the optical case. The constants t_0 and m are determined by the same least squares iteration procedure as previously employed.[4] The results are listed in Table II. The values of $f_e(\Lambda)$ and $\varphi_e(\Lambda)$ obtained through this procedure were subsequently used to construct equilibrium Mooney–Rivlin plots (eq 3). A nonlinear least squares iteration[4] was used which allows the determination of not only the constants G^*, C_1^*, C_2^*, A^*, A_1^*, and A_2^* but also the initial, unstrained length L_0. The 5-min, 1-hr, and equilibrium values of these constants are listed for all 13 samples in Table I.

It is clear from Table II that all $m^{(m)}$ values are essen-

TABLE II
OPTICAL AND MECHANICAL TIME-DEPENDENT CHARACTERISTICS OF PHEMA HYDROGELS

Sample no.	$t_0^{(m)}$, sec	$m^{(m)}$	$t_0^{(o)}$, sec	$m^{(o)}$	Log $a_x^{(m)}$	Log $t_0^{(m)}/t_{03}^{(m)}$	Log $a_x^{(o)}$	$h^{(o)}/h^{(m)}$
1	5.2×10^4	0.135			2.65	2.71		
2	1.6×10^4	0.139			2.20	2.20		
3	1.0×10^2	0.150	2.9	0.165	0	0	0	0.567
4	1.3×10^1	0.156	3.2×10^{-1}	0.159	−1.10	−0.90	−0.75	0.555
5	3.1	0.151	6.0×10^{-2}	0.155	−1.65	−1.52	−1.55	0.538
6	0.81	0.147	4.8×10^{-2}	0.156	−2.10	−2.10	−1.70	0.635
7	7.1×10^{-2}	0.139	8.5×10^{-3}	0.150	−3.00	−3.15	−2.40	0.713
8	8.5×10^{-3}	0.156	3.0×10^{-3}	0.160	−4.15	−4.08	−3.15	0.845
9	1.0×10^{-3}	0.165	8.1×10^{-4}	0.170	−5.10	−5.01	−3.81	0.966
10	3.1×10^{-4}	0.170	2.0×10^{-4}	0.177	−5.80	−5.52	−4.25	0.934
11	8.0×10^{-5}	0.180	8.0×10^{-5}	0.180	−6.35	−6.11	−4.55	1
12	1.0×10^{-5}	0.185	1.0×10^{-5}	0.185	−7.25	−7.01	−5.35	1
13	1.0×10^{-6}	0.200	1.0×10^{-6}	0.200	−8.45	−8.01	−6.20	1

tially independent of the stage of dilution during network formation and independent of the cross-linker concentration. Furthermore, Figure 2 shows that at higher cross-linker concentrations (c) the time dependencies $f_2(t) = f/f_e$ are closer to equilibrium; increasing dilution during network formation seems to decrease effectively c. These observations allow us to use a superposition procedure, similar to a procedure for creep in rubbers used by Plazek.[9] We define an apparent molecular weight between cross-links

$$M_{app} = RTq^{-1/3}\rho_d/(C_1(\infty)^* + C_2(\infty)^*) \quad (10)$$

In those cases where C_2^* is absent we replace $C_1^* + C_2^*$ by G^*; ρ_d is the equilibrium density of the dry network. Figure 4 shows the master curve obtained by shifting the lines in Figure 2 to an arbitrary reference sample (no. 3) by amounts log $a_x^{(m)}$; Figure 5 shows log $a_x^{(m)}$ *vs.* M_{app} defined by eq 10. The master curve over more than 12 decades can be described by eq 9 with $m^{(m)} = 0.152$ and $t_{03}^{(m)} = 1.2 \times 10^2$. Figure 6 shows the characteristic plot[4] for the validity of eq 9. The $m^{(m)}$ and $t_{03}^{(m)}$ compare well with the respective values in Table II. The constancy of $m^{(m)}$ indicates that to a good approximation log $a_x^{(m)}$ = log $(t_0^{(m)}/t_{03}^{(m)})$, where $t_0^{(m)}$ and $t_{03}^{(m)}$ are the constants for the sample which is shifted and the reference sample, respectively.

For the time dependencies of the extinction angle

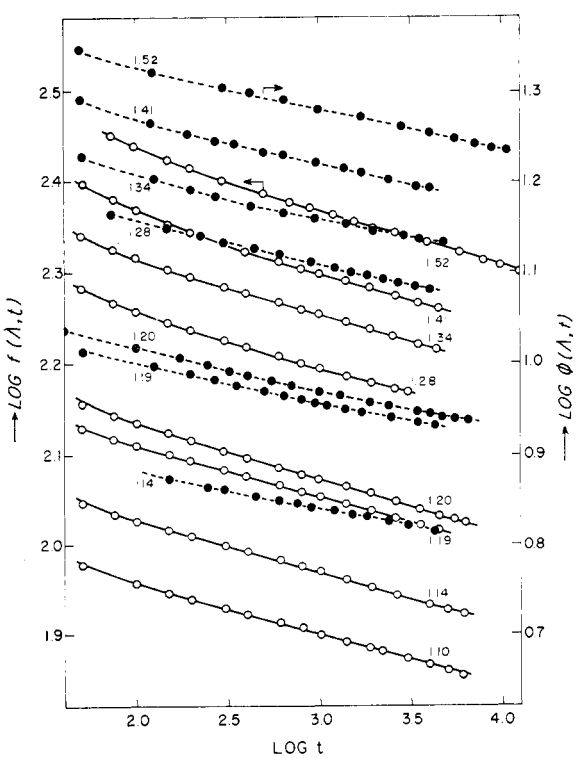

Figure 1. Experimental values of force f in grams (○) and extinction angle φ in degrees (●) *vs.* time (seconds) for sample no. 3. The numbers in the graphs refer to the elongation ratios Λ.

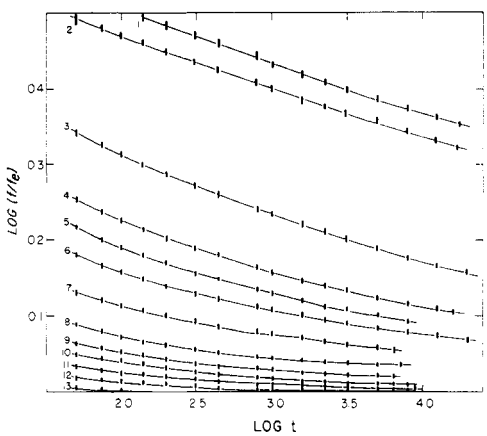

Figure 2. Time-dependent part of the force, $f_2 = f/f_e$, *vs.* time (seconds) for all hydrogels. The numbers refer to the samples in Table I.

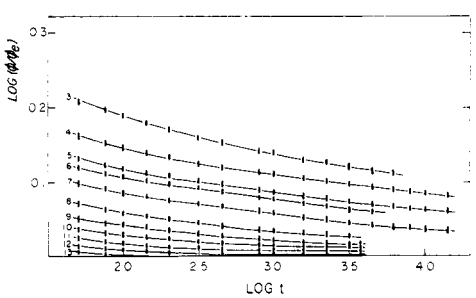

Figure 3. Time-dependent part of the extinction angle $\varphi_2 = \varphi/\varphi_e$ *vs.* time (seconds) for all hydrogels. The numbers refer to the samples in Table I.

(9) D. J. Plazek, *J. Polym. Sci., Part A-2*, 4, 745 (1966).

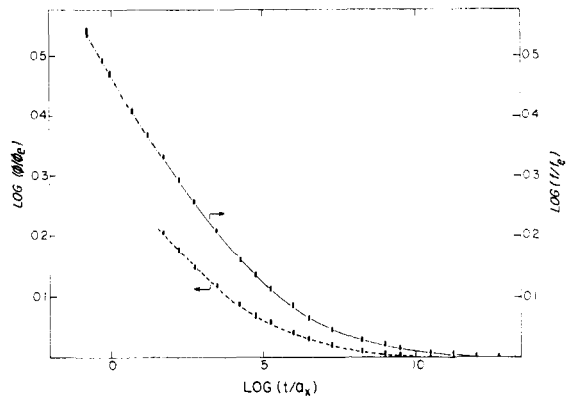

Figure 4. Superposed time dependence of the force, f/f_e (drawn line), and extinction angle, φ/φ_e (dashed line), *vs.* reduced time t/a_x; a_x refers to $a_x^{(m)}$ and a $a_x^{(o)}$, respectively. As reference sample no. 3 is chosen.

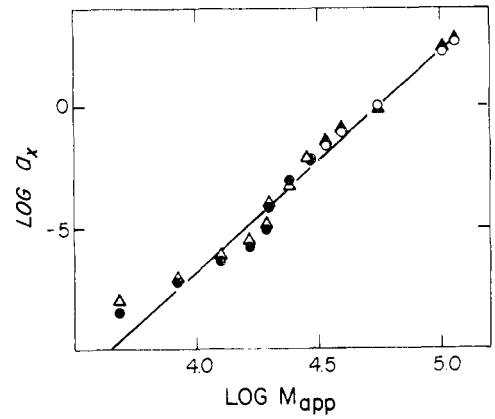

Figure 5. Dependence of the mechanical shift factor, a_x, on the apparent molecular weight between permanent junctions, M_{app} (eq 10). Samples 1–5, experimental values (○), $t_0^{(m)}/t_{03}^{(m)}$ values (▲); samples 6–13, experimental values (●), $t_0^{(m)}/t_{03}^{(m)}$ values (△).

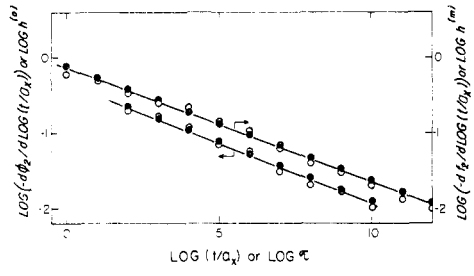

Figure 6. First approximation mechanical and optical relaxation spectra or test of eq 9 (○) and exact spectra (●) *vs.* reduced time $t/a_x = \tau$.

$\varphi_2(t) = \varphi/\varphi_e$ an analogous analysis can be made (Figures 3 and 4). The shift factor $a_x^{(o)}$ differs in this case from the previous mechanical shift $a_x^{(m)}$ (Table II) because the optical data are closer to equilibrium. In Figure 4, a_x refers to $a_x^{(o)}$ and $a_x^{(m)}$, respectively. It is found (see Table II) that the optical values, $m^{(o)}$, are about the same as the mechanical, $m^{(m)}$, but that the $t_0^{(o)}$ constants differ from $t_0^{(m)}$ at larger M_{app} values. The master curve is characterized by $m^{(o)} = 0.158$ and $t_{03}^{(o)} = 3.3$ (see Figure 6).

The differences in $t_0^{(m)}$ and $t_0^{(o)}$ lead to a time dependence in the stress-optical coefficient $C(t) = \Delta n(t)/\sigma(t)$. The equilibrium stress-optical coefficients C_e, obtained from $f_e(\Lambda)$ and $\varphi_e(\Lambda)$, are shown in Figure 7 in which the time dependencies are also indicated.

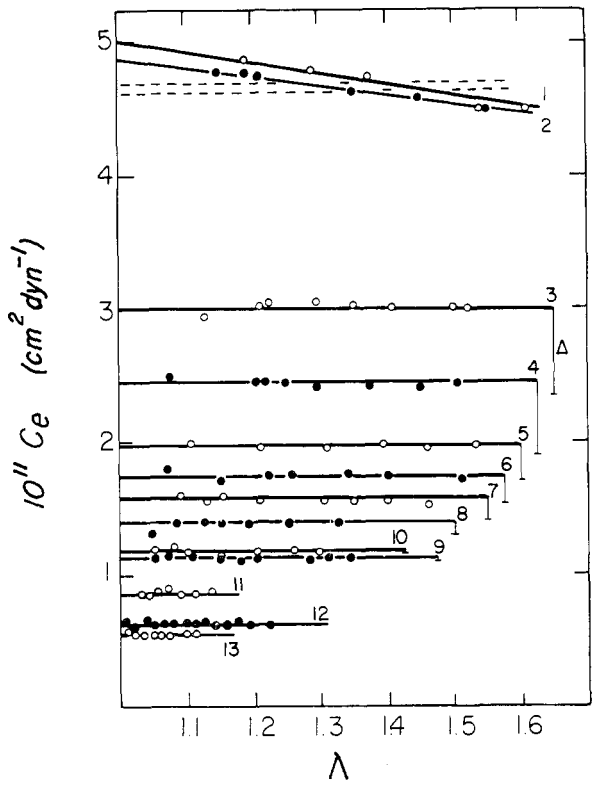

Figure 7. Extrapolated equilibrium stress-optical coefficients, C_e, *vs.* the elongation, Λ, for all hydrogels. The numbers refer to the samples in Table I: Δ indicates the change in $\Delta n/\sigma$ from 5 min to equilibrium.

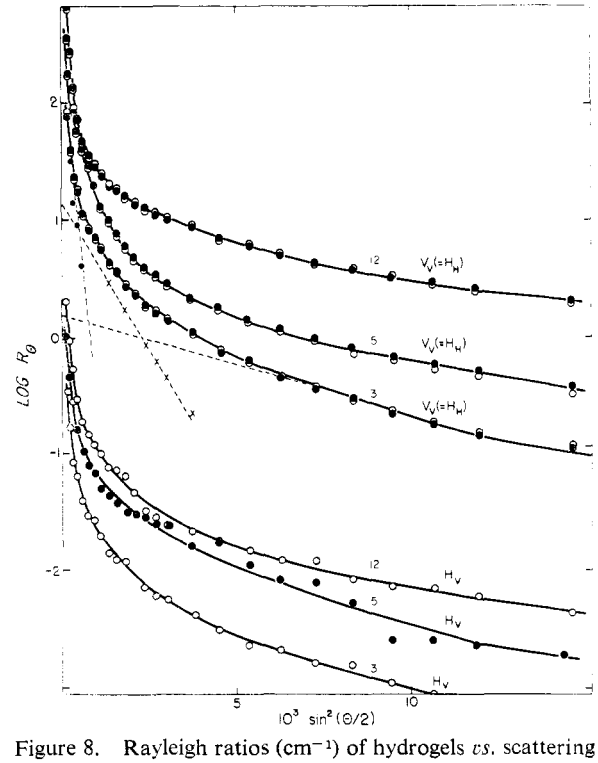

Figure 8. Rayleigh ratios (cm^{-1}) of hydrogels *vs.* scattering angle θ. The numbers refer to the samples in Table I.

The small-angle light-scattering intensities H_v, V_v,

and H_h show angular dependencies characteristic of long-range correlations. Some examples are given in Figure 8. The refractive indices of the gels are all about equal to 1.43–1.44 because the swelling is roughly the same for all samples. Using the same evaluation procedure as before,[4] we find that most of the H_v scattering derives from a 5000 Å correlation.

Mechanical and Optical Relaxation in the Rubbery Region. Mechanical Spectrum. Since the experimental results have yielded the analytical expression for $f_2(t)$ given by eq 9, we can insert this in eq 2 and obtain the inverse Laplace transform

$$h^{(m)} = [2.303/\Gamma(m)](t_0^{(m)}/\tau)^m \quad (11)$$

where $\Gamma(m)$ is the gamma function. It should, of course, be remembered that this spectrum $h^{(m)}$ is only valid in the range covered by the master curve, which is located at times above the main glass–rubber transition. The superposition of Figure 4 shows that in this terminal region the shape of the spectrum does not depend on the stage of dilution during network formation or on the cross-linking density. In the preceding article we have noted that the shape of the spectrum was also independent of the equilibrium degree of swelling. An independence of the shape of the compliance on cross-linking density has previously been observed for the creep behavior of natural rubber vulcanizates.[6] We have[10]

$$j_2(t) = \frac{\sin m\pi}{m\pi f_2(t)} \quad (12)$$

where $j_2(t)$ is the function of time which characterizes the time dependence of the compliance; m is the slope of $\log [f_2(t) - 1]$ *vs.* $\log t$. Since $m \approx 0.15$ we can reduce eq 12 to $j_2(t) = 1/f_2(t)$ with 5% accuracy. Furthermore

$$j_2(t) = j_g + \int_{-\infty}^{+\infty} l^{(m)}(1 - e^{-t/\tau})\, d\log\tau \quad (13)$$

where j_g is the instantaneous contribution; $l^{(m)}$ is the reduced mechanical retardation spectrum, for which we have

$$\int_{-\infty}^{+\infty} l^{(m)}\, d\log\tau = j_e - j_g$$

where $j_e = 1/f_e = 1$. Thus

$$j_2(t) = \frac{1}{1 + (t_0^{(m)}/t)^m} = 1 - \int_{-\infty}^{+\infty} l^{(m)} e^{-t/\tau}\, d\log\tau \quad (14)$$

Since $t_0^{(m)}/t < 1$ in most experimental cases, we have

$$(t_0^{(m)}/t)^m(1 - (t_0^{(m)}/t)^m + \ldots) = \int_{-\infty}^{+\infty} l^{(m)} e^{-t/\tau}\, d\log\tau \quad (15)$$

so that in first approximation $l^{(m)} = h^{(m)}$ in this τ domain. Thus Plazek's retardation spectrum can be compared with our relaxation spectrum. For both there is a region of at least ten decades in which the spectrum can be represented by a straight line with a slope $0.1 < m < 0.2$. Stress relaxation data of Chasset and Thirion[11] also yield values for m in the same region. We conclude that there exists a large region of τ where $\log h^{(m)}$ (or $l^{(m)}$) has a characteristic slope of $0.1 < m < 0.2$ which does not depend on the network parameters or on the chemical nature of the polymer. In this (terminal) region it is only the distance from final equilibrium, governed by the value of M_{app}, that determines the time-dependent behavior. With decreasing M_{app} any interchain interaction (for example, entanglements) should become more and more restricted so that the longer relaxation times will vanish from the spectrum (and can reappear as a contribution to the equilibrium modulus).

The same conclusion follows from the M_{app} reduction scheme used in Figures 2–5. The dependence of the shift factor a_x on the value of M_{app} cannot be interpreted in terms of increasing friction (decreasing free volume). Instead it could be related to the gradual elimination of long-range motions of chain entanglements between cross-links.[9] In Figure 5 it is seen that the cross-linking density as well as the dilution during network formation influences the shift factor only through the value of M_{app}, which represents a molecular weight between permanent cross-links (possibly including some entanglements) in equilibrium.

This part of the mechanical behavior is thus very similar to that of rubber vulcanizates. There is no necessity at this point to invoke mechanisms other than those due to restrictive interactions of chemical cross-links on the response of a transient entanglement network.

The value $m^{(m)} \approx 0.15$, which holds regardless of the network formation parameters and appears to be valid for several polymers, deserves some further comment. For a chemically cross-linked network Chompff and Duiser[12] have shown that the single-molecule Rouse spectrum of slope $-m^{(m)} = -0.5$, immediately above the onset of the main transition, should be followed by a region in which the slope is -1.0. For entanglement networks[13] the CD theory leads to the prediction that the single-molecule Rouse region with slope -0.5 is followed at larger relaxation times by a new region again with slope -0.5. The case of interpenetrating entanglement and permanent networks has not yet been considered. Simple addition of the two spectra will not do since that will never lead to a slope of about -0.15. By adjusting the slip parameter δ in the CD theory to reflect entanglement restriction between cross-links, it may be possible to derive the spectrum of a chain carrying entanglements between cross-links and to employ subsequently this spectrum in the series summation for the spectrum of the permanent network.[12] Theoretical work along this line is in progress in our laboratories.

Optical Spectrum. Although the slopes $m^{(o)}$ of the

(10) H. Leaderman in "Rheology," Vol. II, F. R. Eirich, Ed., Academic Press, New York, N. Y., 1958.

(11) R. Chasset and P. Thirion, Proceedings of the International Conference on Non-Crystalline Solids, North Holland Publishing Co., Amsterdam, 1965.

(12) A. J. Chompff and J. A. Duiser, *J. Chem. Phys.*, **45** 1505 (1966).

(13) A. J. Chompff and W. Prins, *ibid.*, **48**, 235 (1968).

optical relaxation spectra log $h^{(o)}$ (see eq 2 and 9) are about the same as the slopes $m^{(m)}$ of the mechanical spectra, there are important differences in the $t^{(o)}$ and $t_0^{(m)}$ values (Table II); for the higher values of M_{app} we find $t_0^{(o)} < t_0^{(m)}$, which means that the optical spectra are shifted backward with respect to the mechanical. The lower the value of M_{app} the closer the optical and mechanical relaxation are to equilibrium (see Figures 2 and 3). Differences in $t_0^{(o)}$ and $t_0^{(m)}$ are finally no longer discernible. It is worthwhile to point out that $t_0^{(o)}$ becomes equal to $t_0^{(m)}$ at the value of M_{app} (= 10,000) at which also C_2^* in eq 3 becomes zero.

The backward shift of $h^{(o)}$ with respect to $h^{(m)}$ leads to a time dependence of the stress–optical coefficient. This is indicated in Figure 7 where Δ denotes the change of $\Delta n/\sigma$ from its 5-min value to its extrapolated equilibrium value. In the preceding article[4] the spectral differences were in a very general way connected with two main processes: during stress relaxation one not only loses a certain amount of chain orientation, but also creates some new birefringence proportional to the loss of stress at a given time due to a restructuring in the strained network. This was formulated by writing

$$\Delta n(t) = \Delta n^{(c)}(t) + \Delta n^{(nc)}(t) \qquad (16)$$

where $\Delta n^{(c)}(t)$ is the Rouse-type configurational relaxation of the chains—which leads to a time-independent stress–optical coefficient—and $\Delta n^{(nc)}(t)$ is the nonconfigurational ("restructuring") part. The experimental finding that $h^{(o)} \propto h^{(m)}$ leads to a simplication in the treatment of eq 16, which results in the following expression for the time dependence of the stress–optical coefficient[4]

$$C(t) = \frac{\Delta n(t)}{\sigma(t)} = C_e \frac{\left[1 + \int_{-\infty}^{+\infty} h^{(o)} e^{-t/\tau}\, d\log\tau\right]}{\left[1 + \int_{-\infty}^{+\infty} h^{(m)} e^{-t/\tau}\, d\log\tau\right]} = C_e \frac{\left[1 + K\int_{-\infty}^{+\infty} H_\tau e^{-t/\tau}\, d\log\tau\right]}{\left[1 + (\Delta\sigma/\sigma_e)\int_{-\infty}^{+\infty} H_\tau e^{-t/\tau}\, d\log\tau\right]} \qquad (17)$$

where H_τ (= $h^{(m)}(\sigma_e/\Delta\sigma)$) is the normalized logarithmic relaxation spectrum, $\Delta\sigma = \sigma(0) - \sigma_e$, and $K = \Delta\sigma(C^{(c)} - C^{(r)})/\Delta n_e$. The spectral ratio[4] for $m^{(m)} = m^{(o)} = 0.16$ is

$$h^{(o)}/h^{(m)} = \sigma_e(C^{(c)} - C^{(r)})/\Delta n_e = [t_0^{(o)}/t_0^{(m)}]^{0.16} \qquad (18)$$

with $C^{(c)}$ and $C^{(r)}$ the configurational and restructuring parts of the stress optical coefficient. With decreasing M_{app} the ratio $h^{(o)}/h^{(m)}$ approaches unity (see Table II). Equations 17 and 18 show that only if $h^{(o)}$ equals $h^{(m)}$ or $C^{(r)} = 0$ do we obtain a time-independent stress–optical coefficient. Experimentally we cannot ascertain whether indeed $h^{(o)} = h^{(m)}$ at small M_{app} values because such samples are very close to equilibrium in our static relaxation experiments. If one recognizes that $C^{(c)}$ should not depend on M_{app} according to the Gaussian network theory, then the picture of the structure arrived at in the preceding article can be expanded as follows: with increasing M_{app} the amount of restructuring taking place in the network increases, whereas at lower M_{app} the restructuring is impeded so that ideal Gaussian behavior is approached. Figure 7 shows that indeed the time dependence in $\Delta n/\sigma$ disappears at high cross-linking and low dilution during network formation. Assuming $C^{(r)}$ to approach zero at small M_{app}, Figure 9 allows us to estimate $C^{(c)}$. We find $C^{(c)} \approx 0.5 \times 10^{-11}$ cm^2 deg^{-1} or $\Delta\alpha_e = 1.3 \times 10^{-25}$ cm^3 (from eq 7). This value is the same as found for sample 5 swollen in ethylene glycol,[4] which has the same refractive index as the present sample 13 in water. Obviously the increased swelling in ethylene glycol has the same effect on C_e as the increased cross-linking, in accord with our model. Consequently, the changes in C_e with M_{app} in Figure 9 can be attributed to changes in $C^{(r)}$, which reflects the restructuring.

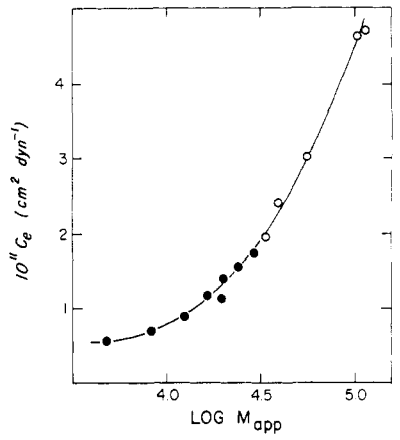

Figure 9. Dependence of the equilibrium stress–optical coefficient, C_e, on the apparent molecular weight between permanent network junctions, M_{app}. Samples 1–5 (○), samples 6–13 (●).

Mechanical and Optical Equilibrium Behavior. The equilibrium stress and birefringence for most of our samples fit the Mooney–Rivlin equations (eq 3) much better than the Gaussian equations (4). For the higher cross-linking densities the range of Λ values that could be covered before breakage of the sample occurred was sometimes too small to allow the construction of a MR plot. In those cases eq 4 was employed instead. Table I lists the G^*, C_1^*, C_2^*, A^*, A_1^*, and A_2^* values obtained in this way, as calculated from the extrapolated equilibrium stress as well as from the 5-min and 1-hr data. Although the errors in C_2^* are large it appears that C_2^* is roughly constant, whereas C_1^* decreases with time.[14] It is interesting to note that C_2^*/C_1^* decreases smoothly with decreasing M_{app}. If C_2^* is associated with the existence of entanglements, the above finding is understandable, because at low M_{app} the entanglements act more and more as permanent cross-links.

In spite of the deviation from Gaussian behavior which makes the molecular meaning of the C_1^* and C_2^* constants uncertain, one can calculate an elastically effective number of network chains, ν^*, from, for example, $C_1^* + C_2^*$ by applying eq 5 and comparing

(14) This behavior is contradictory to the experimentally found separability of the stress in a deformation and time-dependent part (compare eq 1, 2, and 3), but in accord with the previously found[2] temperature independence of C_2^*. As it is uncertain anyway, we will leave this behavior unexplained.

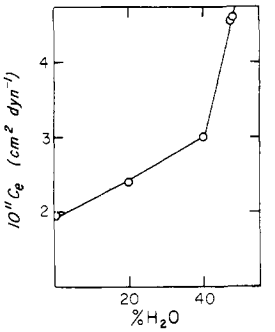

Figure 10. Dependence of the equilibrium stress–optical coefficient, C_e, on the weight per cent water during network formation.

these ν^* values with the theoretical number of chains between chemical cross-links, which is equal to $2c$. This provides information about the number of entanglements and the efficiency of the cross-linking reaction. With increasing cross-linker concentration ν^* increases. Similarly ν^* decreases with increasing stage of dilution during network formation. These conclusions are in accord with previous papers,[2,15] where only 5-min modulus data were obtained.

Whereas the mechanical equilibrium data thus do not require recourse to any structure beyond the existence of cross-links and entanglements, the optical behavior indicates that there must be more to it. The coefficient $(A_1^* + A_2^*)$ rises much more slowly with the number $2c$ than the corresponding $C_1^* + C_2^*$. Also $A_1^* + A_2^*$ does not decrease with the stage of dilution during network formation as does $C_1^* + C_2^*$. As a result the equilibrium stress–optical coefficients, C_e, shown in Figure 9 depend strongly on the network formation conditions as expressed by M_{app}. This is contradictory to the predictions of Gaussian network theory (eq 7), which stipulates that C_e should be independent of cross-linking density as well as of the stage of dilution during network formation. If we plot C_e for a given cross-linking density (c 0.065 $\times$ 10^{-4} mol/cm³) but for different stages of dilution during network formation (Figure 10), we find a very clear break at 45% H_2O. This corresponds to the critical dilution above which microphase separation sets in due to incompatibility of the water with the polymer network. At the same time the gel becomes visibly turbid. It seems logical to connect this high C_e value with the change in structure due to the phase separation. Below the critical dilution the increase of C_e with increasing M_{app} can be readily understood in terms of the restructuring hypothesis which also explained the time-dependent optical properties as described in the previous section. The amount of restructuring leading to nonconfigurational birefringence buildup is then seen to be more pronounced at large M_{app} values, probably because higher dilution during cross-linking and lower cross-linking density both lead to less impedance toward interchain correlations.

For the following reasons the nature of the birefringence should at least partly be form birefringence which changes with M_{app}. The swelling is in all samples low and about the same, as is their refractive index. Macroform birefringence of Gaussian chains should be absent at these low degrees of swelling; microform birefringence of the individual chain segments may exist but should be the same in all samples. The light scattering (Figure 8) shows that there is intrinsic anisotropy present in the samples, but that it is decreasing with increasing M_{app}. The intrinsic anisotropy may be connected with the chain segments and cross-links themselves, but the experimentally found angular dependence of the light scattering indicates that there must also be long-range orientational correlation between chains. The total anisotropic scattering, extrapolated to zero scattering angle, can then be written as in eq 8. Since we expect the volume fraction occupied by anisotropic interchain correlated regions to diminish with decreasing M_{app}, the increasing anisotropic scattering must be ascribed to the increasing cross-linking which raises ϕ_x and ϕ_c.

Thus we have to conclude finally that the larger values of C_e at larger M_{app} where the intrinsic anisotropy is lower must be due to increased form birefringence which can only arise from changes in the interchain correlated regions, which re-form themselves during stress relaxation after their (partial) destruction at the beginning of the experiment. The form birefringence indicates that the interchain regions are anisometric and differ in refractive index from their surrounding.

Conclusions

The preceding article stated the case for a certain amount of structuring and restructuring in PHEMA gels in a series of diluents, including water. The present results confirm the previous conclusions for a series of water-swollen PHEMA gels in which two network formation parameters were widely varied.

It was found that the stage of dilution and the cross-linking density affect the structural, mechanical, and optical properties of the resulting networks through a single parameter, *viz.*, the apparent molecular weight between cross-links as calculated from eq 10. For a qualitative understanding of the time-dependent mechanical behavior, a structural picture consisting of cross-links and entanglements is sufficient.

The differences between the optical and mechanical relaxation spectra in the rubbery region increase with increasing M_{app}, leading to a time-dependent stress–optical coefficient, whereas the Rouse-type relaxation of the chains between chemical cross-links should lead to a time-independent stress–optical coefficient.[5]

The equilibrium stresss–optical coefficient increases about ninefold with an increase of M_{app} from about 3000 to 8000, whereas in a Gaussian network that coefficient should be constant.

The light-scattering data on unstrained gels point toward the existence of anisotropic regions of interchain correlation of the order of 5000 Å, roughly independent of the value of M_{app}.

The above optical results can be explained by reference to the restructuring process given in the previous paper.[4] Upon deformation there is a partial or complete destruction of organized regions, followed by a restructuring during stress relaxation. An examina-

(15) J. Janacek and J. Hasa, *Collect. Czech. Chem. Commun.*, 31, 2186 (1966); J. Hasa and J. Janacek, *J. Polym. Sci., Part C*, 16, 317 (1967).

tion of the equilibrium stress-optical coefficients in connection with the light-scattering results shows that the reorganized regions should exhibit a higher form anisotropy the larger the value of M_{app}. Such increasing form anisotropy can be either due to increasing anisometry of the regions or—at a given anisometry—due to an increasing refractive index difference with the surrounding.

The reasons for the appearance of some fairly long-range anisotropic structures in the PHEMA hydrogels have previously, in the first place, been traced to the amphiphilic nature of the polymer chain, which especially in water could lead to regions of micromesomorphic order.[4] Inhomogeneous cross-linking may be a second contributing factor, especially if water is present during network formation.

The optical behavior can be qualitatively understood in terms of a somewhat organized network containing cross-links and entanglements. Any cross-link or entanglement will restrict the long-range organization. The movement of entanglements during stress relaxation will change the interchain correlations, so that a restructuring will result. At small M_{app} the equilibrium optical behavior will approach the Gaussian behavior because the large number of cross-links disrupts the organizing tendency of the amphiphilic system.

Acknowledgments. The financial support of the Syracuse University Research Institute is gratefully acknowleged. M. I. expresses his gratitude to the Institute of Macromolecular Chemistry, Czechoslovak Academy of Sciences, for granting a leave of absence, which made his postdoctoral stay in the U. S. possible. J. Hasa, Prague, has kindly cooperated in the preparation of the samples.

Light Scattering from a Two-Phase Polymer System. Scattering from a Spherical Domain Structure and Its Explanation in Terms of Heterogeneity Parameters[1a]

Masahiko Moritani,[1b] Takashi Inoue, Masahiko Motegi,[1c] and Hiromichi Kawai[1d]

Department of Polymer Chemistry, Faculty of Engineering, Kyoto University, Kyoto, Japan. *Received February 16, 1970*

ABSTRACT: The correlation function $\gamma(r)$ defined by Debye and Bueche for characterizing the inhomogeneity of solid materials is further investigated by measuring the intensity distribution of scattered light under the V_v polarization condition from the film specimens of block copolymers of styrene and isoprene (A–B type) and graft copolymers of butadiene and styrene–acrylonitrile (ABS resin type). Three kinds of heterogeneity parameters, "specific surface" S_{sp}, "distance of heterogeneity" $\bar{l}_e$, and "volume of heterogeneity" $\bar{\nu}$, as well as some statistical parameters, such as "short- and long-range correlation distances" a_1 and a_2 and "fractional contribution factors of short- and long-range fluctuations" f and $(1 - f)$, are determined from the intensity distribution of scattered light from the specimens, and are discussed in relation to the heterogeneity of the spherical domain structures of the specimens observed from their electron micrographs.

The heterogeneity in the structure of polymer solids greatly influences the bulk properties, and the light scattering may be a useful technique for quantifying the heterogeneity of the same dimensional order as the wavelength of the light used.

The theoretical studies of the light scattering from solid materials were first carried out by Debye and Bueche[2a] for an isotropic but inhomogeneous system, made more general by Goldstein and Michalik,[2b] and further extended by Stein and his coworkers[3–6] to the anisotropic system of crystalline polymers. In accordance with these theories, the intensity distribution of scattered light could give some statistical parameters which are related to the fluctuations of optical density and orientation within the system, *i.e.*, the heterogeneity and local anisotropy. However, the physical meaning of the parameters in relation to the heterogeneity of the system has not been fully understood, except for, for example, some indirect investigations where the parameters are compared with the results obtained from adsorption experiments.[7] This may be due to the lack of test specimens appropriate for making direct comparison of the parameters with the heterogeneity of the system.

Recent developments of synthesizing block and graft copolymers have made it possible to control the microphase separations of the block segments and of the grafted and backbone segments during casting the

(1) (a) Part of M.S. Thesis of M. Moritani presented to the Department of Polymer Chemistry, Faculty of Engineering, Kyoto University, March 10, 1970; presented partly before the 18th Annual Meeting of the Society of Polymer Science, Japan, Kyoto, May 20, 1969. (b) Niihama Mill, Shumitomo Chemical Co., Ltd., Niihama, Ehime-ken, Japan. (c) Film Laboratory, Toyo Rayon Co., Ltd., Ohtsu, Shiga-ken, Japan. (d) To whom all correspondence should be addressed.

(2) (a) P. Debye and A. M. Bueche, *J. Appl. Phys.*, **20**, 518 (1949); (b) M. Goldstein and E. R. Michlik, *ibid.*, **26**, 1450 (1955).

(3) R. S. Stein and M. B. Rhodes, *ibid.*, **31**, 1873 (1960).

(4) R. S. Stein and P. R. Wilson, *ibid.*, **33**, 1914 (1962).

(5) R. S. Stein, P. R. Wilson, and S. N. Stidham, *ibid.*, **34**, 46 (1963).

(6) R. S. Stein, P. Erhardt, J. J. van Aartsen, S. Clough, and M. B. Rhodes, *J. Polym. Sci., Part C*, **13**, 1 (1966).

(7) P. Debye, H. R. Anderson, and H. Brumberger, *J. Appl. Phys.*, **28**, 679 (1957).